Algorithms for the computation of solutions of the Ornstein-Zernike equation

A. T. Peplow*
Department of Mathematics, Imperial College, 180 Queen's Gate, South Kensington, London, SW7 2AZ, United Kingdom

R. E. Beardmore†
Department of Mathematics, Imperial College, 180 Queen's Gate, South Kensington, London, SW7 2AZ, United Kingdom

F. Bresme‡
Department of Chemistry, Imperial College, South Kensington, London, SW7 2AZ, United Kingdom

(Received 6 March 2006; revised manuscript received 2 August 2006; published 17 October 2006)

We introduce a robust and efficient methodology to solve the Ornstein-Zernike integral equation using the pseudoarc length (PAL) continuation method that reformulates the integral equation in an equivalent but nonstandard form. This enables the computation of solutions in regions where the compressibility experiences large changes or where the existence of multiple solutions and so-called branch points prevents Newton's method from converging. We illustrate the use of the algorithm with a difficult problem that arises in the numerical solution of integral equations, namely the evaluation of the so-called *no-solution line* of the Ornstein-Zernike hypernetted chain (HNC) integral equation for the Lennard-Jones potential. We are able to use the PAL algorithm to solve the integral equation along this line and to connect physical and nonphysical solution branches (both isotherms and isochores) where appropriate. We also show that PAL continuation can compute solutions within the *no-solution region* that cannot be computed when Newton and Picard methods are applied directly to the integral equation. While many solutions that we find are new, some correspond to states with negative compressibility and consequently are not physical.

DOI: 10.1103/PhysRevE.74.046705 PACS number(s): 05.10.−a, 05.50.+q, 02.70.−c

I. INTRODUCTION

The Ornstein-Zernike (OZ) relation represents a powerful approach to investigating the structure and thermodynamics of condensed phases [1]. Different closures must be augmented with the OZ relation in order to obtain a problem that is soluble and for the case of the hypernetted chain (HNC) closure it has been noted that the resulting equation exhibits a forbidden region where no physical real solutions are found for certain density and temperature conditions [2–6].

This so-called *no-solution region* has been taken as an approximation to the liquid-vapor coexistence curve in the past, although it has also been noted in the cited numerical studies that it does not always appear to be connected to a divergence of isothermal compressibility, as should be observed when approaching a coexistence region.

The divergence of the isothermal compressibility that defines the spinodal line *is* observed in some integral equations, such as the mean spherical approximation (MSA) [7]. In this particular instance, it has been pointed out that the numerical solution of the integral equation can differ from the analytical result unless the numerical solution is obtained with great care, see also Ref. [8]. Even more dramatically, an integral equation that bears a formal resemblance to OZ-HNC has been constructed in Ref. [9] in such a way that there is absolutely no correspondence between the solutions of the integral equation and the solutions of its discretization. This may be a problem when solving integral equations such as OZ-HNC and when using interatomic potentials such as the Lennard-Jones, since these theories can only be solved using a numerical approach.

We should like to point out there are three issues regarding the accurate computation of solutions of any nonlinear integral equation: (1) how that equation is discretized, (2) how that discretization is solved subject to a suitably small error tolerance, and (3) how well the numerically computed solutions actually approximate a true solution of the underlying equation. This paper only concerns problem (2) from this list, although our discretization method from step (1) is a slight improvement on the standard one in that convolutions are computed in a manner that is equivalent to replacing the trapezium rule with Simpson's rule. Problem (3) is a problem in theoretical numerical analysis that is not addressed here at all.

Our *numerically obtained* solutions of the OZ-HNC integral equation suggest that the *no-solution line* results from the divergence of two square root branch points and the subsequent existence of multiple solutions [2]. In Ref. [10] it is argued that the existence of this behavior in the numerical realization of the OZ-HNC equation is logically consistent with the existence of a true spinodal in the OZ-HNC equations. Another study [4] argues that the *no-solution region* is connected to the onset of complex solutions, although this property is simply a consequence of the existence of branch points.

In this paper we discuss a very general methodology that has existed for over 30 years in the numerical mathematics literature [11] and apply it to the Ornstein-Zernike equation. We illustrate its use with the HNC closure, but we would like to emphasize that the method is completely general and can

*Electronic address: a.peplow@ic.ac.uk
†Electronic address: r.beardmore@ic.ac.uk
‡Electronic address: f.bresme@ic.ac.uk

be used with other closures too. One of our aims is to develop a method that is robust in the vicinity of the no-solution line and in regions where compressibility exhibits large changes, including divergence due to the existence of a critical region.

There are a number of algorithms that are suitable for such bifurcation problems. One of these is the pseudoarc length (PAL) continuation method and we show that the implementation of this method and the reformulation of the HNC integral equation in a nonstandard manner results in an efficient methodology that can be easily employed to investigate the no-solution line. This method resolves many of the deficiencies associated with Newton and Picard methods and enables one to find solutions that cannot be found using the latter methods directly.

The structure of the paper is as follows. First we introduce the problem and briefly discuss the origin of the limitations of the traditional Newton method when applied to problems with branch points. There follows a discussion of the numerical implementation of the arc-length continuation method and we then present our results for the OZ-HNC integral equation using the Lennard-Jones potential, our conclusions close the paper.

II. THE ORNSTEIN-ZERNIKE EQUATIONS, NEWTON'S ALGORITHM AND BIFURCATIONS

The Ornstein-Zernike (OZ) equation with hypernetted chain (HNC) closure is the following problem: find functions h and c such that

$$h(r) - c(r) = \rho \int_{\mathbb{R}^3} h(\|x-y\|)c(\|y\|)dy, \tag{1}$$

$$h(r) = -1 + e^{-\beta u(r)} e^{h(r)-c(r)}. \tag{2}$$

Here x and y are vectors in three-dimensional space, $r=\|x\|$ is the radial coordinate where $\|(x_1,x_2,x_3)\|=(x_1^2+x_2^2+x_3^2)^{1/2}$ is Euclidean distance, ρ is the mean particle density, $\beta=1/(k_BT)$ is the Boltzmann factor, T the temperature, and $u(r)$ is the intermolecular potential. The total (h) and direct (c) correlation functions yield the indirect correlation function $\gamma=h-c$ and, using this definition, Eqs. (1) and (2) can be rewritten as a single integral equation of the form

$$\gamma = \rho[f + e^{-\beta u}(\exp\ \gamma - 1)] * [f + e^{-\beta u}(\exp\ \gamma - 1) - \gamma], \tag{3}$$

where $f(r)=-1+e^{-\beta u(r)}$ is the Mayer f-function and $*$ denotes convolution.

Isothermal compressibility κ_T is defined by

$$\kappa_T = \left[(\rho k_B T)\left(1 - 4\pi\rho \int_0^\infty r^2 c(r)dr \right) \right]^{-1}, \tag{4}$$

the value of which is obtained numerically by evaluating $\int_0^R r^2 c(r)dr$ for a *large* value of R and when plotting the results of computations we shall use the normalized inverse compressibility χ^{-1}, where

$$\chi = \frac{1}{1 - 4\pi\rho \int_0^\infty r^2 c(r)dr} = 1 + 4\pi\rho \int_0^\infty r^2 h(r)dr. \tag{5}$$

The OZ-HNC equation may therefore be written as a single equation of the form

$$\gamma = \rho N(\gamma, \beta), \tag{6}$$

where N is a suitably defined nonlinear function, which is convenient for the presentation of numerical algorithms. For instance, the Picard method is given by

$$\gamma_{n+1} = \rho N(\gamma_n, \beta), \quad \gamma_0 \text{ an initial guess}, \tag{7}$$

and this algorithm is assured to converge if $\rho>0$ is sufficiently small. However (6) will not converge if ρ nears the critical density.

Preliminary: Newton's algorithm and bifurcations. The OZ equation coupled with any closure relation is an example of a nonlinear integral equation that one cannot solve analytically for most intermolecular potentials. Its solution structure possesses subtleties that depend on the choice of potential and on physical parameters such as density and temperature. Moreover, as those parameters are varied the number of solutions of the equations changes. The mathematical parlance for the parameter value at which such a change is observed is called a *bifurcation point*; this paper is a response to the need for a numerical code that can locate bifurcations or spinodals (which *is* a type of bifurcation) of the OZ-HNC equation in an automated fashion, given that Newton's method alone applied to the OZ equation can locate neither bifurcation points nor spinodals.

Newton's method is designed to solve a very general, possibly high-dimensional equation of the form

$$F(\gamma) = 0, \tag{8}$$

by taking an initial guess γ_0 and refining through the sequence of iterates defined by

$$\gamma_{n+1} = \gamma_n - dF(\gamma_n)^{-1} F(\gamma_n). \tag{9}$$

In fact this process is commonly used in studies of the OZ equation, but the algorithm requires a fundamental property to hold so that the sequence of iterates (γ_n) can be obtained: at a solution γ^* whereby $F(\gamma^*)=0$, it must be the case that the matrix of partial derivatives of $F(\gamma)$ at $\gamma=\gamma^*$, denoted $dF(\gamma^*)$, is an *invertible* or *nonsingular* matrix (one that has a nonzero determinant). Note that A^{-1} is used here and throughout to denote the inverse of a matrix A.

However, if F is used to represent the OZ equation with HNC closure then Newton's method *will not work* near a candidate spinodal or near the critical region because the matrix $dF(\gamma^*)$ will *always* turn out to be singular in this region. Picard iterations are also commonly used in the literature, but these are just special cases of Newton iterations and so they will not work in these regions.

In order to obtain as much detail of the solution structure as possible, we adopt the pseudoarc-length (PAL) strategy that is due to Keller and others that is now a common tool in bifurcation analysis within the scientific community [12,11].

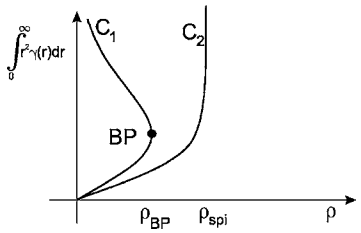

FIG. 1. Schematic of a branch point, fold bifurcation or pseudospinodal in C_1 and an isothermal solution branch C_2 with a spinodal.

Indeed, these techniques have already been used in a density-functional framework, as can be seen in Ref. [13] whose authors emphasize the need for the application of bifurcation-based tools in the study of integral equation theories of phase transitions.

Before continuing, we remark that the *continuation method* described in Ref. [14] is termed *natural parameter continuation* in the numerical analysis literature and what we propose is quite different. Also, the term *continuation method* is often used for any algorithm that can cope with the presence of bifurcations and other instabilities.

In this paper we explain how one can alter the formulation of Newton's method to locate *spinodals* if they are present, to locate *pseudospinodals*, a term that is defined below, and to find the location of pseudospinodals as a function of temperature and density. The algorithms are relatively fast in the sense that they run in Matlab on a single processor Pentium 4(2.6 GHz, 2 GB RAM) machine with up to 2^{18} mesh points, using the fast-Fourier transform (in the west) FFTw to implement convolution and we use the matrix-free linear solver GMRES that is available as a standard part of the Matlab environment in order to find the Newton updates as defined in (9). To locate a single solution takes of the order of seconds to minutes, depending on the size of the numerical mesh used for the computations.

For illustrative purposes we have presented two scenarios in Fig. 1 that would prevent Newton's algorithm from converging when applied to the OZ-HNC equation: one (C_1) is a *branch point, fold bifurcation or pseudospinodal* (terms that we consider to be synonymous, although we prefer the term branch point) that is not associated with the divergence of compressibility but is related to a numerical instability because compressibility is large in some sense; and another (C_2) is a *spinodal* along which compressibility does diverge. The former is so named because of the folded geometry of the solution curve near the point BP and this arises because *two* solutions of the equations are present for $0 \leqslant \rho < \rho_{\mathrm{BP}}$.

It is near the label BP that Newton's method would fail because if ρ were just a little less than ρ_{BP}, the fact that two solutions are to be found so close to each other creates a vertical tangent at BP that causes a numerical instability for (9). A similar comment applies to the isothermal solution branch C_2 where the instability arises because of the asymptotically vertical tangent of the graph at the spinodal.

III. LOCATING A SPINODAL: THE PROBLEM

When seeking a spinodal of the OZ-HNC equation, we require solutions that satisfy the condition

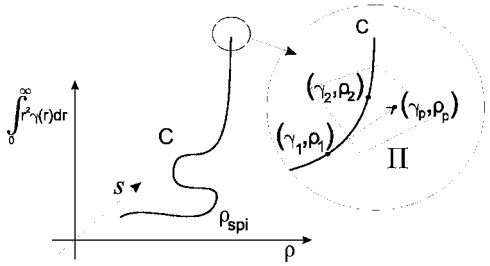

FIG. 2. Consider a known solution (γ_1,ρ_1) on a near-spinodal isothermal solution branch C. In order to locate the solution (γ_2,ρ_2), begin by finding the tangent direction of the curve at (γ_1,ρ_1) and use this to locate a suitable nearby initial guess or *linear predictor* (γ_p,ρ_p). Now use (γ_p,ρ_p) as an initial guess for a Newton iteration whose iterates remain in the plane Π and converge to (γ_2,ρ_2); the normal vector of Π is the previously computed tangent direction.

$$1 - 4\pi\rho \int_0^\infty r^2 c(r) dr = 0. \tag{10}$$

However, a solution pair (h,c) of (1) and (2) that satisfies (10) also satisfies $\int_0^\infty r^2 h(r) dr = \infty$ and so can be shown to be associated with an inherent numerical instability.

It therefore seems natural to try and locate a spinodal by obtaining solutions of (1) and (2) at low density to begin with, which can be done very easily using a Picard iteration for any potential and temperature. Then, by slowly increasing density and holding temperature fixed, one can track the branch of isothermal solutions as closely as possible to a desired spinodal.

However, this approach is doomed to fail if one uses an unmodified Newton method on (1) and (2) because of the high sensitivity of the solutions to changes in density as one nears the spinodal. One must therefore reduce the incremental changes in density in a fashion that is commensurate with the increases in the integral of h and γ as one nears a branch point or a spinodal.

In Refs. [2–6] the authors have applied a bare Newton method (although sometimes the authors use Picard methods) to study the number of solutions of the OZ equations. While such an approach will be successful away from the critical region, as temperature nears its critical value for, say, a Lennard-Jones fluid, Newton methods applied to OZ with any closure must cease to converge. Below the critical temperature, a Newton method will also fail unless the values of the density parameter are carefully chosen to ensure that the solution one is seeking is some way away from any spinodal or pseudospinodal that may be present.

A. Locating a spinodal: the solution

In order to compute as close to a spinodal as possible we undertake the following operation that is depicted in Fig. 2. The procedure begins by treating OZ-HNC (or OZ with any closure) as an equation not just for the correlation function γ but one also considers ρ to be an unknown, but temperature is held at a fixed value.

Thus we have the equation $\gamma=\rho N(\gamma,\beta)$ with two unknowns γ and ρ. We now augment this problem with a new equation and therefore replace Eq. (6) with the pair

$$G(\gamma,\rho,s) := (\gamma-\rho N(\gamma,\beta),\alpha(\gamma,\rho,s)) = (0,0), \qquad (11)$$

where we have added a new unknown s and an auxiliary function α. The function α merely serves as a way of parametrizing any solution curve of (6) in (γ,ρ)-space with the auxiliary parameter s that acts as an arc-length variable for this purpose. In [15,11] one can find the mathematical details of how and why this is done.

There are two points two be made: first, by a judicious choice of α we will be able to solve Eq. (11) for (γ,ρ) as a function of the artificial parameter s; second, we shall do this in such a way that Eq. (11) can be solved *even when one cannot* solve (6) easily using Newton's method for the unknown γ. The reason for this is that Newton's method can fail to find solutions even when they are there; this is not a purely numerical issue but one associated with a change in the solution structure of the underlying equations. Typically, when two solutions are too close together to allow a sufficiently good initial guess to be found then Newton cannot easily proceed as this closeness property renders the linear system in the Newton iteration numerically ill conditioned or near singular. Precisely this situation occurs at a branch point of the OZ-HNC equations.

The point is that when applying a Newton method to (6), the inherent instability of being close to a spinodal forces a numerical instability that renders the linear system within the Newton iteration [given by (9)] a singular linear system. However, one can choose α in such a way that when applying a Newton method to (11), the associated linear system of *that* Newton method *is* nonsingular.

Figure 2 gives a geometric description of this method. Given a solution γ_1 at $\rho=\rho_1$ on a solution curve C, so that $\gamma_1=\rho_1 N(\gamma_1,\beta)$ and (γ_1,ρ_1) is a vector pair that lies on C, one predicts where a nearby solution on the solution branch will be located by looking a small distance, ds say, along the tangent direction of the curve. This gives an initial guess or *predictor* (γ_p,ρ_p) for a Newton method that is constructed in such a way that the iterates of that method lie within a plane Π whose normal direction coincides with the previously computed tangent direction. This Newton method is iterated to convergence in order to locate (γ_2,ρ_2) and the use of the tangent vector along C automatically adjusts for the fact that the curve *steepens* in the sense that the size of $d\gamma/d\rho$ increases along C near the spinodal.

In order to complete the description of the methodology we must provide the form of the function α in (11). This we do in the next section.

B. Arc-length continuation

As C is a one-dimensional curve we may parametrize it by arc-length s. In principle, there are many possible choices for the function α in (11), but the one used in practice is the linearized or pseudoarc-length constraint given by (again see Ref. [11])

$$\alpha(\gamma,\rho,s) = \mathbf{s}_0\cdot(\gamma-\gamma_0)+\sigma_0(\rho-\rho_0)-(s-s_0),$$

where a dot denotes the inner product of two vectors, as in $(x_1,x_2,\ldots,x_n)\cdot(y_1,y_2,\ldots,y_n)=\sum_{i=1}^{n}x_i y_i$. Moreover, $(\mathbf{s}_0,\sigma_0)$ is the unit tangent vector at a given point on the solution curve C and we assume the existence of a known solution on C so that $G(\gamma_0,\rho_0,s_0)=0$, where G is defined in (11).

The full algorithm thus has the following steps, where ds assumes a *fixed, small* value:

(P1) Choose ρ_0 to be sufficiently small that Picard iteration will converge, set $s_0=0$ and find $(\gamma_0,\rho_0)\in$ C using Picard.

(P2) Given a solution $(\gamma_k,\rho_k)\in$ C at the arc-length parameter s_k, let $s_{k+1}=s_k+ds$ and find the unit tangent vector to C by solving the linear system of equations

$$\partial_\gamma G(\gamma_k,\rho_k,s_k)\bar{\gamma}+\partial_\rho G(\gamma_k,\rho_k,s_k)\bar{\rho}=-\partial_s G(\gamma_k,\rho_k,s_k)$$

for $(\bar{\gamma},\bar{\rho})$ and then define a *unit* vector $(\mathbf{s}_k,\sigma_k)$ by

$$\mathbf{s}_k=\frac{\bar{\gamma}}{\sqrt{\|\bar{\gamma}\|^2+\bar{\rho}^2}}, \quad \sigma_k=\frac{\bar{\rho}}{\sqrt{\|\bar{\gamma}\|^2+\bar{\rho}^2}}.$$

(P3) Apply Newton iteration to $G(\gamma,\rho,s)=0$ with initial guesses $\gamma=\gamma_k+ds\cdot\mathbf{s}_k$ and $\rho=\rho_k+ds\cdot\sigma_k$ and denote the solution thus found $(\gamma_{k+1},\rho_{k+1})$.

The algorithm (P1)–(P3) is still based on Newton's method and both steps (P2) and (P3) require the use of a linear solver and one could use, say, Gaussian elimination (or LU decomposition) applied to the derivative matrix of (11). However, this would be *extremely* inefficient as it requires the derivative matrix to be constructed and then inverted, so instead we use the *GMRES algorithm*. As is discussed in Ref. [16], this is appropriate for integral equations like OZ-HNC and has the particular advantage of never needing to form the derivative matrix of (11) when applying Newton's method within the PAL algorithm.

In practice, ds must be chosen small enough so that the Newton iteration described in the preceding paragraph converges. We altered the value of ds so that if this iteration required a small number of Newton steps then ds would be increased by a fixed factor, reducing ds if the number of iterations were too high; this is especially helpful as the algorithm nears a branch point or spinodal. In practice, we used 0.1 for ds when ρ is small, which decreased to as small as $ds=10^{-2}$ or 10^{-3} when passing through branch points.

If ds is sufficiently high and two solution branches are to be found sufficiently close together, this may permit the PAL algorithm to *jump* from one solution branch to another; it is this property that initially lead us to finding solution branches of negative compressibility. However, using the Newton-GMRES code detailed in Refs. [17,16] that has also been written in Matlab, we were in fact able to choose temperature and density within the no-solution region and locate such a nonphysical solution with little difficulty. This is because the Newton algorithm of Refs. [17,16] (that, note, can be downloaded as the Matlab m-file oz.m located at http://www4.ncsu.edu/~ctk/newtony.html) always converges to some solution, irrespective of the density that we chose, and

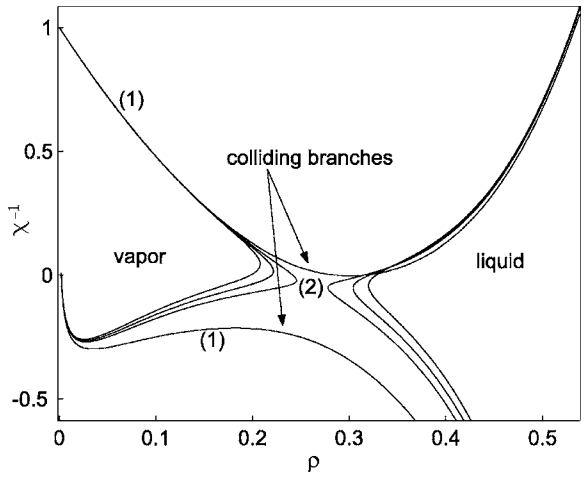

FIG. 3. Four representative isothermal pairs of solution branches where $R=20\sigma$ and $n=2^{10}+1$: the two isotherms labeled (1) are supercritical (both isothermals have been computed with $T^*=1.41$) whereas the others are for subcritical temperatures.

this solution was then continued to form an entire isothermal solution branch using the PAL algorithm.

IV. PSEUDOSPINODALS

One can exploit one of the properties of matrices that leads to nonconvergence of Newton's method (9) in order to track the precise location in the (ρ,β)-plane of where OZ-HNC will possess pseudospinodals. Now, a matrix A is singular if there is a nonzero vector $\mathbf{k}$ such that $\mathsf{A}\mathbf{k}=\mathbf{0}$ and Newton's method applied to OZ-HNC will fail if the matrix of partial derivatives of $\gamma-\rho N(\gamma,\beta)$ is singular when viewed as a function of γ.

We can apply this idea to (3) as follows: let us find (k,γ,ρ) such that

$$\begin{pmatrix} \gamma-\rho N(\gamma,\beta) \\ (I-\rho\partial_\gamma N(\gamma,\beta))k \\ \|k\|^2-1 \end{pmatrix} = \begin{pmatrix} 0 \\ 0 \\ 0 \end{pmatrix}, \tag{12}$$

where A corresponds to the matrix of partial derivatives $I-\rho\partial_\gamma N(\gamma,\beta)$ and I is the identity matrix. The first equation in (12) is a repetition of (3), the second ensures that when Newton's method is applied to (3) it cannot converge: in effect we are using the second equation in (12) to impose the condition that the matrix which is formed from the linearization of the OZ equation (3) is a matrix that possesses a nonzero null vector and is therefore a singular matrix. This is precisely the condition that prevents Newton from converging. The third equation in (12) is the condition that k is nonzero, where $\|k\|^2=\Sigma_{i=1}^n k_i^2$ is used to denote Euclidean distance squared of the vector $k=(k_1,\ldots,k_n)$.

One could reformulate (12) as the following equivalent system of equations:

$$\begin{pmatrix} \gamma-\rho N(\gamma,\beta) \\ \det(I-\rho\partial_\gamma N(\gamma,\beta)) \end{pmatrix} = \begin{pmatrix} 0 \\ 0 \end{pmatrix}, \tag{13}$$

where det denotes the determinant of a matrix. However, (13) would not provide for an efficient numerical implementation due to the presence of the determinant.

By solving (12) one obtains the boundary of theoretical convergence of Newton's method applied to (3) in the (ρ,β) plane which is the locus of branch points. One can apply either a standard Newton method to (12) with β fixed, or one can use the PAL algorithm in case the approximated curve of branch points has a particularly complicated structure; we have used both approaches in practice.

V. NUMERICAL RESULTS

Before we give the results of our numerical computations, one further remark is in order. When seeking approximate

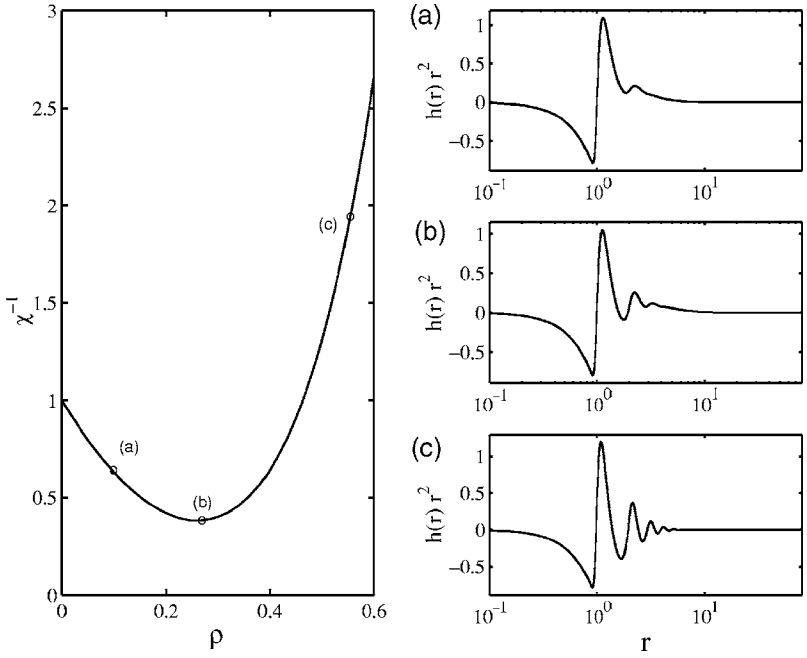

FIG. 4. Inverse isothermal compressibility plotted against density at temperature $T^*=1.6$ for the Lennard-Jones potential (so that T^* is greater than $T_c^*\simeq 1.4$) where $R=80\sigma$ and $n=2^{12}+1$. Three correlation functions, $r^2h(r)$, are presented at density values: (a) $\rho^*=0.1$, (b) $\rho^*=0.270$, and (c) $\rho^*=0.55$.

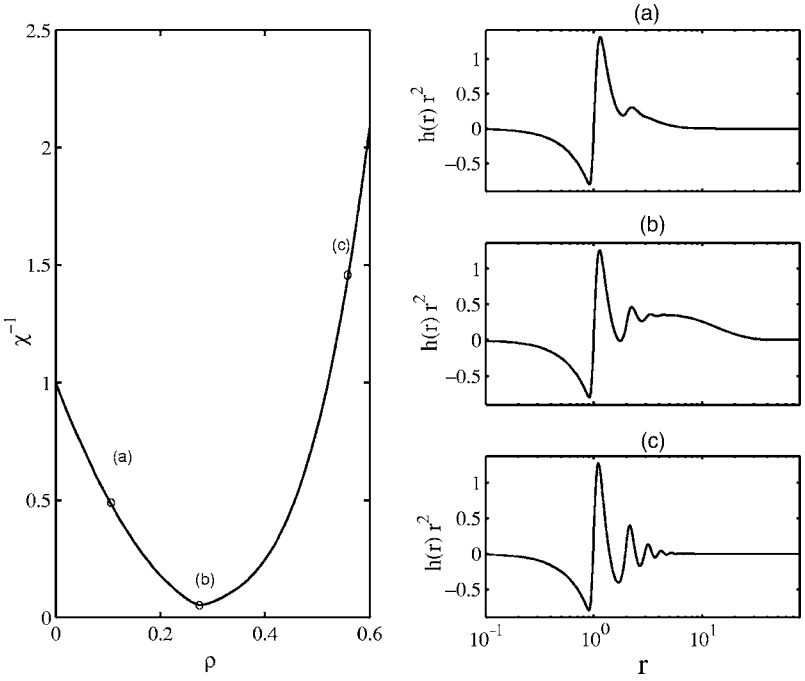

FIG. 5. Inverse isothermal compressibility plotted against density at temperature $T^*=1.408$ (T^* just above T_c^*), for the Lennard-Jones potential, $R=80\sigma$ and $n=2^{12}+1$. Three correlation functions, $r^2h(r)$, are presented at density values: (a) $\rho^*=0.1$, (b) $\rho^*=0.270$ and (c) $\rho^*=0.55$.

solutions of the OZ-HNC equation, the only element of the problem that requires discretization is the convolution operator. To achieve this one uses the fact that convolution can be written using the Fourier transform as

$$a * b = \mathcal{H}^{-1}(\mathcal{H}a\mathcal{H}b), \tag{14}$$

where a,b are two given functions and $\mathcal{H}$ denotes the spherical Hankel transform (the Fourier transform of radially symmetric functions).

It is standard practice in numerical studies of the OZ-HNC equation to truncate the interval of integration in the definition of the Hankel transform to a finite interval $[0,R]$ when solving (1) and (2). So, given that

$$(\mathcal{H}a)(s) = 4\pi \int_0^\infty \mathrm{sinc}(rs) r^2 a(r) dr$$

and the given inverse transform $(\mathcal{H}^{-1}a)(s)=\frac{1}{8\pi^3}(\mathcal{H}a)(s)$, if we define

$$(\mathcal{H}_R a)(s) = 4\pi \int_0^R \mathrm{sinc}(rs) r^2 a(r) dr$$

and $(\mathcal{H}_R^- a)(s)=\frac{1}{8\pi^3}(\mathcal{H}_R a)(s)$, we can formulate the equation that is to be solved numerically using the PAL algorithm,

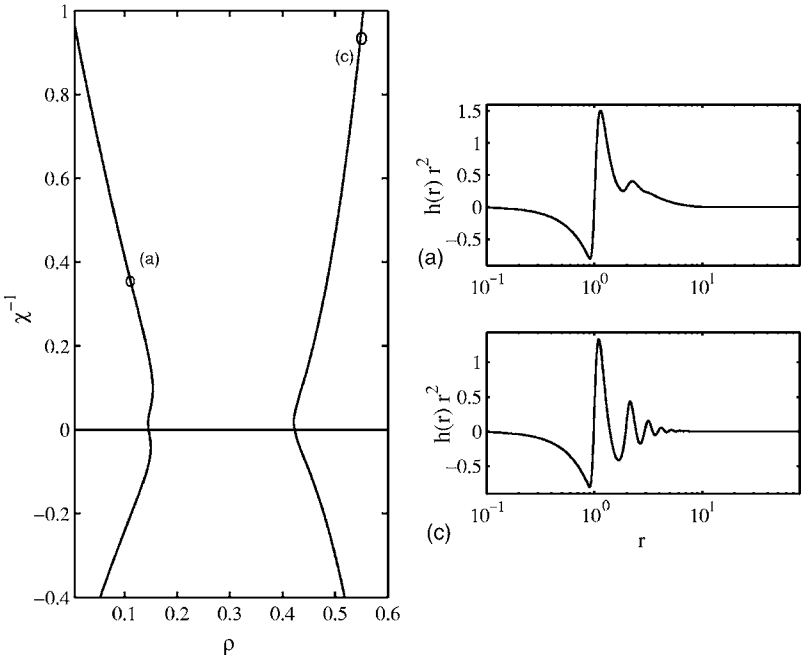

FIG. 6. Inverse isothermal compressibility plotted against density at temperature $T^*=1.3$ (so that $T^*<T_c^*$) for the Lennard-Jones potential with $R=80\sigma$ and $n=2^{12}+1$. Two correlation functions $[r^2h(r)]$ are presented at density values: (a) $\rho^*=0.1$, (b) $\rho^*=0.270$ no solution, and (c) $\rho^*=0.55$.

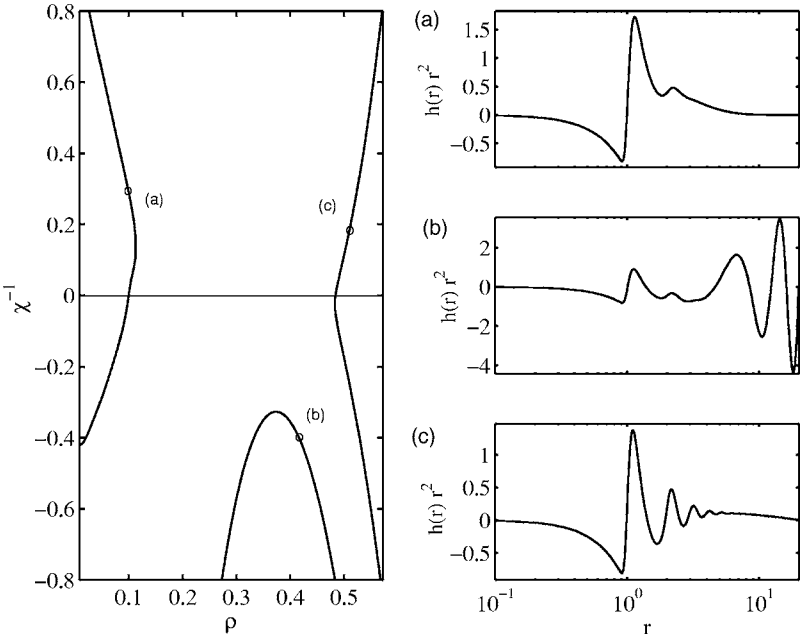

FIG. 7. Inverse isothermal compressibility plotted against density at temperature $T^*=1.2$ for the Lennard-Jones potential, where $R=20\sigma$ and $n=2^{10}+1$. Three solutions, $r^2h(r)$, are presented on each curve at: (a) $\rho^*=0.084$, (b) $\rho^*=0.419$, and (c) $\rho^*=0.509$. Solutions for (a) and (c) are clearly seen to lie on the positive χ-part of the vapor and liquid branches.

$$\gamma = \rho\mathcal{H}_R^-\{\mathcal{H}_R[f+e^{-\beta u}(\exp\gamma-1)] \times \mathcal{H}_R[f+e^{-\beta u}(\exp\gamma-1)-\gamma]\}. \quad (15)$$

In practice we shall solve (15) approximately, exploiting the FFT in our numerical calculations at every opportunity. One significant difference with our discretization (that we do not detail here) and the ones used in all other cited references is the fact that we employ one step of a Richardson extrapolation procedure to obtain $O(n^{-4})$ error estimates for solutions of (15), where n is the numerical mesh size, rather than the $O(n^{-2})$ estimates that are usually obtained. The penalty for this is that while second-order accuracy can be obtain by performing convolution with three FFT operations, our method requires five such operations, but this can be achieved without compromising the $O(n\ln(n))$ complexity of the FFT-based numerical convolution algorithm.

A. Computations

The purpose of this section is to illustrate the applicability of the PAL algorithm (P1)–(P3) to trace solution branches of the OZ-HNC equation with the Lennard-Jones (LJ), double Yukawa (DY), and triple Yukawa (TY) potentials, where the Yukawa potentials are chosen to fit the Lennard-Jones potential. For completeness let us define the Lennard-Jones potential

$$u_{\mathrm{LJ}}(r) = 4\epsilon[(\sigma/r)^{12}-(\sigma/r)^6]. \quad (16)$$

The potential well depth ϵ and the particle diameter σ are used to define the thermodynamic quantities in reduced units,

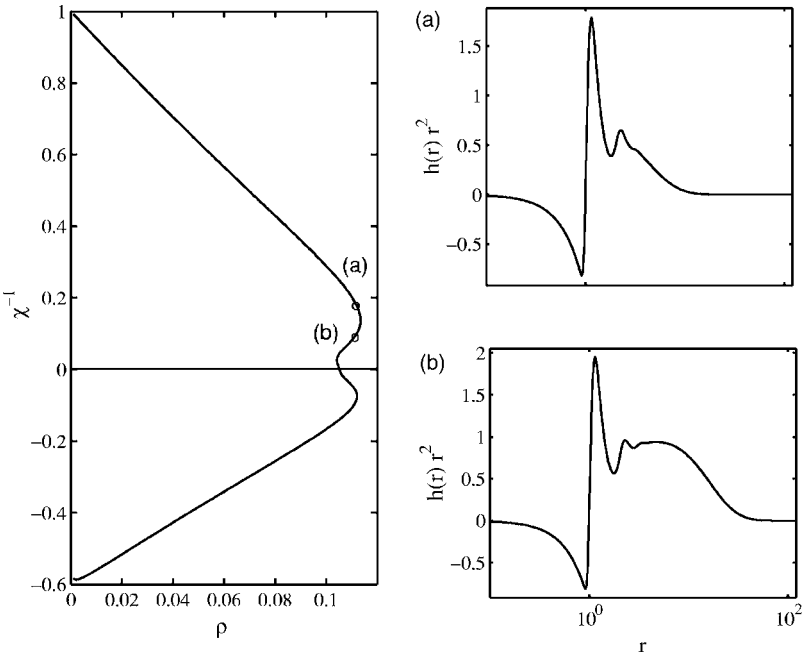

FIG. 8. Inverse isothermal compressibility plotted against density with $T^*=1.2$ for the Lennard-Jones potential, where $R=120\sigma$ and $n=2^{12}+1$. Two solutions, $r^2h(r)$, on each curve are presented at (a) $\rho^*=0.1127$ and (b) $\rho^*=0.1122$. Solution (a) located at upper circle in left-hand plot and (b) located at lower circle.

$\rho^*=\rho\sigma^3$, $T^*=k_BT/\epsilon=1/(\epsilon\beta)$. For the numerical calculations we use a numerical mesh size of $n=2^{12}+1$ points unless otherwise stated. A relative error tolerance of 10^{-11} in the so-called *maximum vector length* or *norm* [18] was used to measure errors for the Newton iterations that were performed.

Our first set of computations is best illustrated by comparing Figs. 3–6, where temperature is held fixed in each computation (at $T^*=1.6$, 1.408, and 1.3, respectively). We have computed the variation of inverse isothermal compressibility with respect to density, ρ^*, as well as the total correlation functions corresponding to three representative thermodynamic states. As the temperature decreases the critical temperature of the Lennard-Jones model is approached and this is reflected in values of the inverse compressibility which develops a minimum at a value of ρ^* somewhere between 0.25 and 0.3.

As temperature is reduced further, Fig. 6 illustrates the creation of two disconnected solution branches: vapor at low densities and liquid at high densities. Note the W-shaped nature of the vapor isotherm whereby several apparent branch points are present in the region of zero inverse compressibility. This is the reason for the nomenclature *pseudospinodal* that we have associated with the branch points as χ^{-1} is typically close to zero when they occur. Figure 6 also shows that one can in fact have an apparently genuine spinodal within the HNC approximation in the sense that the compressibility as it is defined in this paper diverges to infinity. This occurs nonetheless in a manner that corresponds to an unphysical variation of compressibility with respect to changes in density.

The results presented above illustrate the power of the numerical approach desribed in this paper. In previous investigations such as Refs. [2,4] the crossing of inverse compressibility from positive to negative values was not reported. In one of these investigations negative compressibilites were reported but these resulted from a complex-valued solution that itself stems from the existence of a branch point. Figure 6 shows that it is perfectly possible to connect the range of negative values with the positive ones in a continuous fashion along isothermal solution branches of real-valued solutions.

One may ask how two solution branches can appear at low temperatures where only one was present at high temperatures. The answer to this lies in the fact that there *is* another solution branch that exists at the parameter values used in Fig. 4, but it is not plotted in this figure for clarity as it only contains solutions of negative compressibility. We have illustrated this phenomenon in Fig. 3 where supercritical and subcritical isotherms are labeled (1) and (2), respectively, note that there are *two* supercritical isotherms labeled (1) that have been computed at $T^*=1.41$, one has positive and one negative compressibility. It may be instructive to compare Fig. 3 with ([5], Fig. 4).

It is very important to realize that the phenomena described in this section are associated with solutions of the numerical or computational realization of the OZ-HNC equations (15) and not necessarily with the OZ-HNC equations themselves; the mathematical reasons for this are explored in detail in Ref. [10]. For example, it is easy to see from the convolution theorem applied to OZ that it is impossible for a continuous solution of (1) to be realized with zero inverse compressibility, yet it is possible to locate continuous solution of (15) with zero inverse compressibility. This comment is central to the design of qualitatively correct discretization methods for the OZ equation with its various closures, but the analysis that leads to such methods is beyond the scope of this paper.

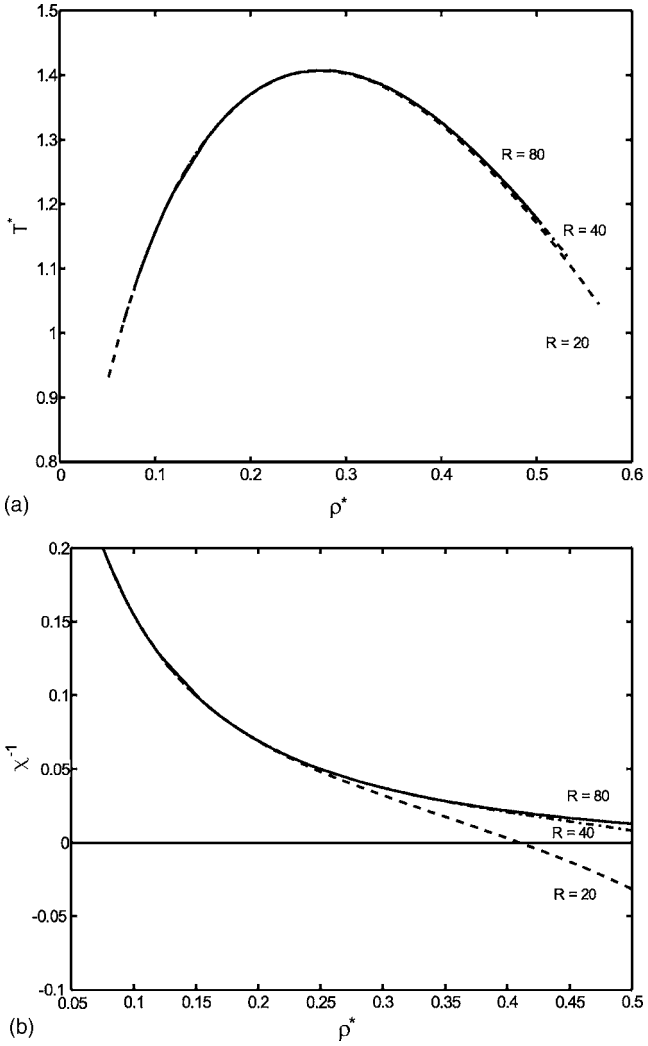

FIG. 9. (a) Locus of branch points and (b) inverse compressibility values for the Lennard-Jones potential for varied cutoff values, R, and $n=2^{12}+1$ points. Legend: $R=80\sigma$ (solid), $R=40\sigma$ (dashed-dotted), and $R=20\sigma$ (dashed line).

Although our next computation has a small numerical mesh with only $n=1025$ points and also has a low cutoff value of $R=20\sigma$ with $T^*=1.2$, we have included it to further illustrate the point made in the preceding section regarding solutions of negative compressibility. One can see in Fig. 7 that we have found many solutions that do indeed have negative compressibility within the so-called no-solution region that are easily located using the PAL algorithm, employing the code from [17] to locate initial points on the branches. The same figure also contains two solution branches of (partially) positive compressibility.

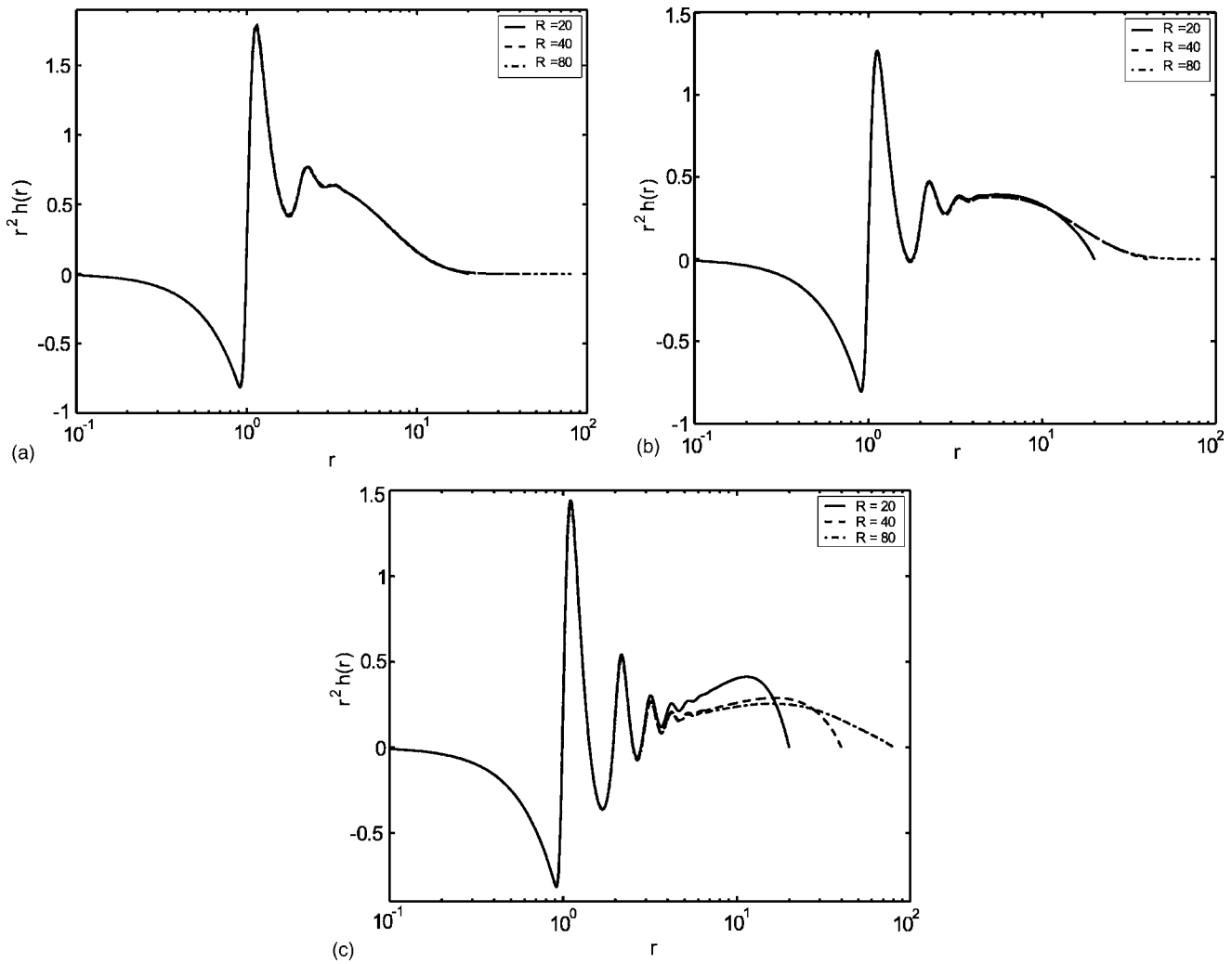

FIG. 10. Distribution functions $r^2h(r)$ at locations along the branch point locus from Fig. 9 for cutoff values $R=20\sigma$, 40σ, and 80σ, using $n=2^{12}+1$ points and the Lennard-Jones potential: $(\rho^*,T^*)=(0.122,1.23)$ (a), (0.275,1.407) (b), and (c) (0.503,1.170). Note that (b) represents solutions at the critical apex of the locus of branch points from Fig. 9.

The correlation function $r^2h(r)$ is indicated in Fig. 7(a) at a point on the vapor isotherm before the first branch point and correlation functions computed on other solution isotherms are also shown. Note in particular Fig. 7(b) showing the unphysical nature of $r^2h(r)$ for large values of r.

The vapor solution branch in Fig. 7 emanates from the point $(\gamma,\rho)=(0,0)$ with unit compressibility and this branch extends to higher densities, but it then continues into the region of negative compressibility at around $\rho=0.12$. It has been reported in the literature that compressibility remains finite in numerical computations when approaching the no-solution region [2,3,5,14,6], indicating that this region is *not* linked to a phase transition. Our computations indicate that in fact there *are* numerical solutions that have zero inverse compressibility, but that they occur on isothermal solution branches beyond the first branch point.

Figure 8 illustrates the effect of increasing the cutoff R. In this case we have used $n=2^{12}+1$ and $R=120\sigma$; this plot refines the left-hand branch shown in Fig. 7. It is important to note that the increase in accuracy has resolved a number of branch points that were missed when using too coarse a mesh in Fig. 7, leading to a W-shaped solution branch with three pseudospinodals. This is reminiscent of behavior found by Belloni for different potentials [2]. The right-hand plots show the total correlation functions of two solutions that are located at the same density either side of a branch point, (a) is a perfectly feasibly physical solution, whereas (b) is not.

Note that we have illustrated solutions that are situated precisely upon the branch point itself in Fig. 10 of the next section and in Fig. 12 at the end of the paper for computations undertaken for the Yukawa potentials.

Figure 9(a) shows a computed locus of branch points as defined in Sec. IV, that is, the locus corresponds to the density-temperature pairs for which a branch point is observed and this curve coincides with the one obtained using different algorithms in Ref. [4].

While the form of this branch point locus is similar for all of the cutoff values $(R=20\sigma,40\sigma,80\sigma)$ that we choose, the values taken by χ^{-1} along this locus are sensitive to R, as can be seen in Fig. 9(b). Each of the curves should, ideally, be very close to zero but they are in fact both above and below zero, depending on the density. The reason for this can be seen in Figs. 6 and 7 where the branch point on the vapor

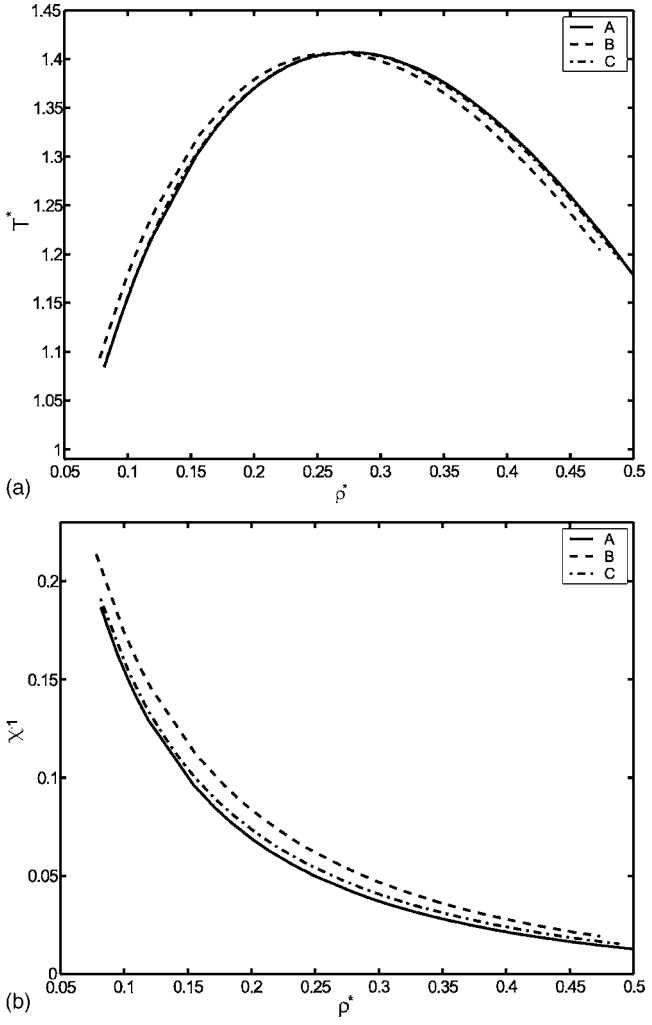

FIG. 11. (a) Locus of branch points for the (A) Lennard-Jones, (B) double Yukawa, and (C) triple Yukawa potentials for cutoff value $R=80\sigma$ and $n=2^{12}+1$ points. (b) Inverse compressibility values along the above locus of branch points for LJ, DY, and TY potentials.

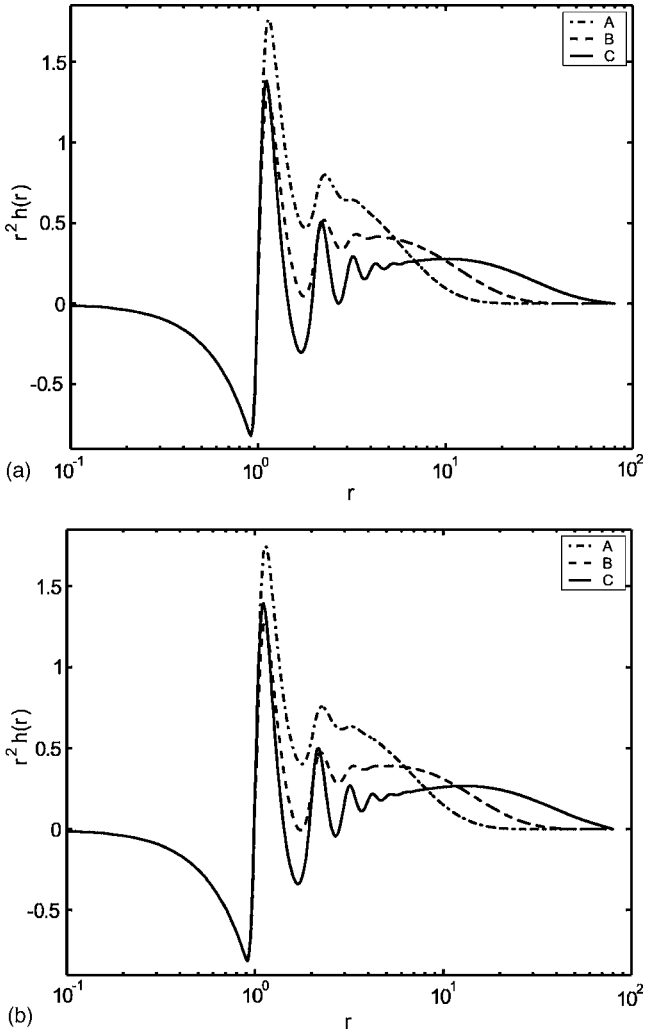

FIG. 12. Plots of $r^2h(r)$ at various locations along the two-parameter branch point locus from Fig. 11 for the DY(a) and TY(b) potentials: $(\rho^*,T^*)=(0.122,1.23)$ (A), (0.275,1.407) (B), and (0.480,1.210) (C). Label (B) represents solutions at the apex of the branch point locus from Fig. 11(a).

branch occurs at positive compressibility before a spinodal is observed, whereas the branch point on the liquid branch occurs at negative compressibility, after an apparent spinodal has already been observed.

Examples of the total correlation functions $r^2h(r)$ computed along the two-parameter parabolic curve from Fig. 9 are presented in Fig. 10: (A) represents solutions in the vapor region, (B) is at apex from Fig. 9(a), and (C) is representative of the liquid region. It is clear in Fig. 10(c) that liquid solutions are particulary sensitive to the cutoff value R, although vapor and near-critical solutions are not affected to the same extent.

B. Double Yukawa and triple Yukawa potentials

We also considered the double Yukawa potential (DY) and triple Yukawa potentials, respectively, (17) and (18) below. The parameters used in (17) taken from [19] are $A_1=1.6438\sigma$, $z_1=14.7\sigma^{-1}$, $A_2=2.03\sigma$, and $z_2=2.69\sigma^{-1}$; we recall that $\sigma=1$ is used throughout. Similarly, the parameters for the triple Yukawa potential are $c_1=2.351\sigma$, $z_3=13.446\sigma^{-1}$, $c_2=0.910$, $z_4=3.482\sigma^{-1}$, and $z_5=1.317\sigma^{-1}$ in (18). In contrast to the Lennard-Jones potential which has algebraic decay, the double Yukawa and triple Yukawa potentials decay exponentially and are given as follows:

$$u_{\mathrm{DY}}(r)=\frac{\epsilon}{r}(A_1e^{-z_1(r-\sigma)}-A_2e^{-z_2(r-\sigma)}) \tag{17}$$

and

$$u_{\mathrm{TY}}(r)=\frac{c_1\epsilon}{r}[e^{-z_3(r-\sigma)}-c_2e^{-z_4(r-\sigma)}-(1-c_2)e^{-z_5(r-\sigma)}]. \tag{18}$$

The purpose of these computations is to compare the loci of branch points of all three potentials and to investigate whether it is the relatively slow decay of the tail of the

Lennard-Jones potential that is responsible for the large values taken by χ^{-1} along this loci as shown in Fig. 9.

The reason for doing this is that this figure gives a measure of how close a branch point or pseudospinodal is to representing a true spinodal. As can be seen in Fig. 11(b), the loci of values taken by χ^{-1} are qualitatively similar for all three potentials, as is the form of the branch point locus shown in Fig. 11(a). We therefore conclude that it is not the slow decay of the tail of the Lennard-Jones potential that leads to the poor approximation of spinodals by branch points. For further comparison with the Lennard-Jones case, we have included Fig. 12 which plots the total correlation functions taken from vapor, critical, and liquid regions of the branch point curve Fig. 11(a) for both double and triple Yukawa potentials.

VI. CONCLUSIONS

We have introduced an automated numerical methodology to solve the Ornstein-Zernike equation at different temperatures and densities and have focused on the HNC closure relation and the Lennard-Jones potential as a case study. We have shown that by employing the pseudoarc-length continuation method one can compute solutions that are not possible to find when applying Newton or Picard methods directly. Moreover, our approach confirms previous analyses of the OZ-HNC equation that have suggested the existence of square root branch points separating physical and unphysical solutions.

One advantage of PAL continuation is that it can pass through branch points in a continuous fashion which represents the main improvement over previous approaches. Interestingly, we have found real solutions within the so-called no solution region. However, the solutions do not connect with the branch points and have negative compressibility and are therefore unphysical.

Moreover, we have been able to compute solutions of zero inverse compressibility on both liquid and vapor branches for potentials with an attractive tail, provided that temperature is sufficiently low. The vapor solution branch shows W- and S-shaped structures at low temperature with as many as three solutions for a given density each with positive compressibility, provided that the cutoff parameter R used in the discretization of (15) is sufficiently large.

[1] J. P. Hansen and I. R. Macdonald, *Theory of Simple Liquids* (Academic, London, 1976).
[2] L. Belloni, J. Chem. Phys. **98**, 8080 (1993).
[3] J. J. Brey and A. Santos, Mol. Phys. **57**, 149 (1986).
[4] E. Lomba and J. L. Lopez-Martin, J. Stat. Phys. **80**, 825 (1995).
[5] P. D. Poll and N. W. Ashcroft, Phys. Rev. A **35**, 5167 (1987).
[6] R. O. Watts, J. Chem. Phys. **50**, 1358 (1969).
[7] P. T. Cummings and G. Stell, J. Chem. Phys. **78**, 1917 (1983).
[8] P. T. Cummings and P. A. Monson, J. Chem. Phys. **82**, 4303 (1985).
[9] C. A. Stuart and G. Vuillaume, Z. Anal. ihre Anwend. **20**, 183 (2001).
[10] R. E. Beardmore, A. T. Peplow, and F. Bresme, http://www.ma.ic.ac.uk/~rebear
[11] H. B. Keller, in *Numerical Solution of Bifurcation and Nonlinear Eigenvalue Problems*, edited by P. Rabinowitz (Academic, New York, 1977).
[12] E. J. Doedel, R. C. Paffenroth, A. R. Champneys, T. F. Fairgrieve, Yu. A. Kuznetsov, B. Sandstede, and X. Wang, Technical Report, Caltech; see also http://indy.cs.concordia.ca/auto/
[13] L. J. D. Frink and A. G. Salinger, J. Chem. Phys. **118**, 7466 (2003).
[14] D. A. Tikhonov and G. N. Sarkisov, Russ. J. Phys. Chem. **74**, 3 (2000).
[15] E. J. Doedel, http://www.cds.caltech.edu/hinke/courses/CDS280/
[16] C. T. Kelley and B. Mongomery-Pettitt, J. Comput. Phys. **197**, 491 (2004).
[17] C. T. Kelley, *Solving Nonlinear Equations with Newton's Method* (SIAM, Philadelphia, 2003).
[18] If $\mathbf{x}=(x_1,x_2,\ldots,x_n)$ then the maximum vector length or norm is $\|\mathbf{x}\|_{\max}=\max_{1\leq i\leq n}|x_i|$.
[19] Elisabeth Scholl-Paschinger, Ph.D. thesis, Intitut fur Theoretische Physik, Vienna, 2002.